Supplementary Information: Characterizing Dark State Kinetics and Single Molecule Fluorescence of FusionRed and FusionRed-MQ at Low Irradiances

Srijit Mukherjee, [1,2] Connor Thomas, [1] Ryan Wilson, [1,3] Emma Simmerman, [4] Sheng-Ting Hung, [5] and Ralph Jimenez [1,2]

[1]JILA, University of Colorado, Boulder and National Institute of Standards and Technology, 440 UCB, Boulder, Colorado 80309, United States

[2]Department of Chemistry, University of Colorado, Boulder, 215 UCB, Boulder, Colorado 80309, United States

[3]Department of Physics, University of Colorado, Boulder, 390 UCB, Boulder, Colorado, 80309, United States

[4]Department of Applied Physics, Stanford University, 348 Via Pueblo Mall, Stanford University, Stanford, CA 94305-4090, United States

[5]Department of Physics, National Sun Yat-sen University, Kaohsiung 80424, Taiwan

Section	Title
S1	*Experimental workflow*
S2	*Excitation rate calculations*
S3	*Single molecule data analysis addendum*
S4	*Ensemble photobleaching*
S5	*Simulation results*
S6	*Statistical testing*
S7	*Additional fitting results*
S8	*Theoretical estimation of the lowest and highest number of photons per frame*
S9	*Surface charge on FusionRed*

S1. Experimental workflow
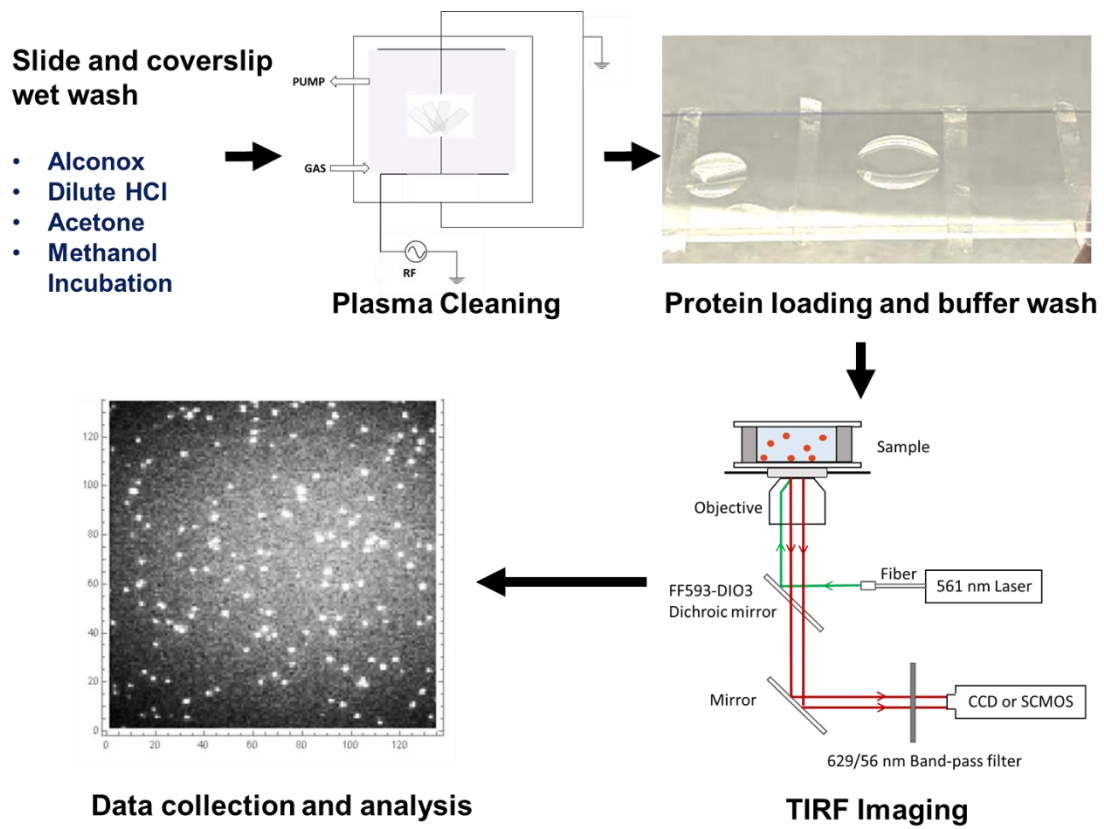
Figure S1.1: Schematic of the experimental workflow from sample preparation to data analysis.

S2. Excitation rate calculations

Our TIRF measurements are for proteins (~1–2 nm) bound to the surface of the coverslip, therefore we estimate the irradiance (I) of the evanescent wave at the interface surface using Fresnel's equations, given below.[1]

$$I_e = I \frac{4(cos\theta)^2(2(sin\theta)^2 - n^2)}{n^4(cos\theta)^2 + (sin\theta)^2 - n^2} \tag{1}$$

$$k_{ex} = \frac{2.303 * I_e * \lambda * \epsilon_\lambda}{ln(2) * N_A * h * c} \tag{2}$$

Table S2.1: Power measurements

Power (mW)	I (W/cm²)	I_e (W/cm²)	Excitation Rate $_{FR}$ (Hz)	Excitation Rate $_{FR\text{-}MQ}$ (Hz)
0.28	0.49	1.23	940	1622
0.42	0.74	1.85	1420	2450
0.49	0.63	1.57	1206	2080
0.56	0.99	2.48	1902	3282
1.24	1.57	3.93	3014	5200
2.48	3.15	7.87	6035	10412
4.96	6.29	15.73	12062	20811

FR = Fusion Red, FR-MQ = FusionRed-MQ

S3. Single molecule data analysis addendum

a. Spot identification script corrections
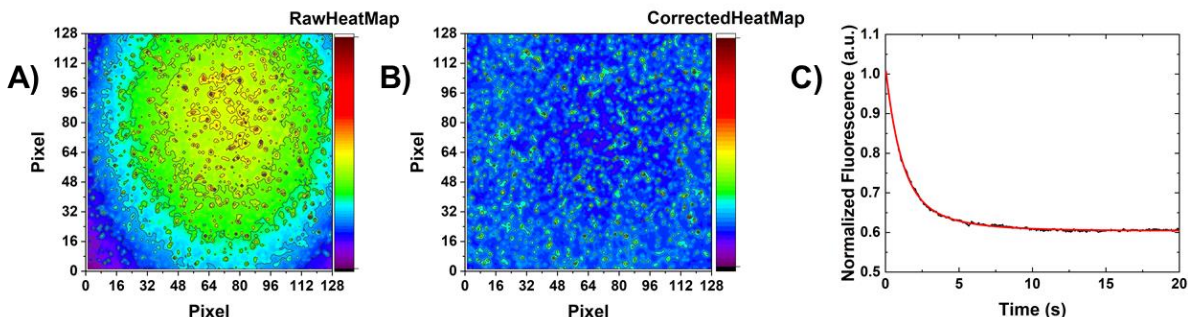
Figure S3.1: Spatial corrections A) Gaussian profile, B) after removal of the Gaussian profile, C) after removal of the fast component on a blank sample.

b. Detection of state changes
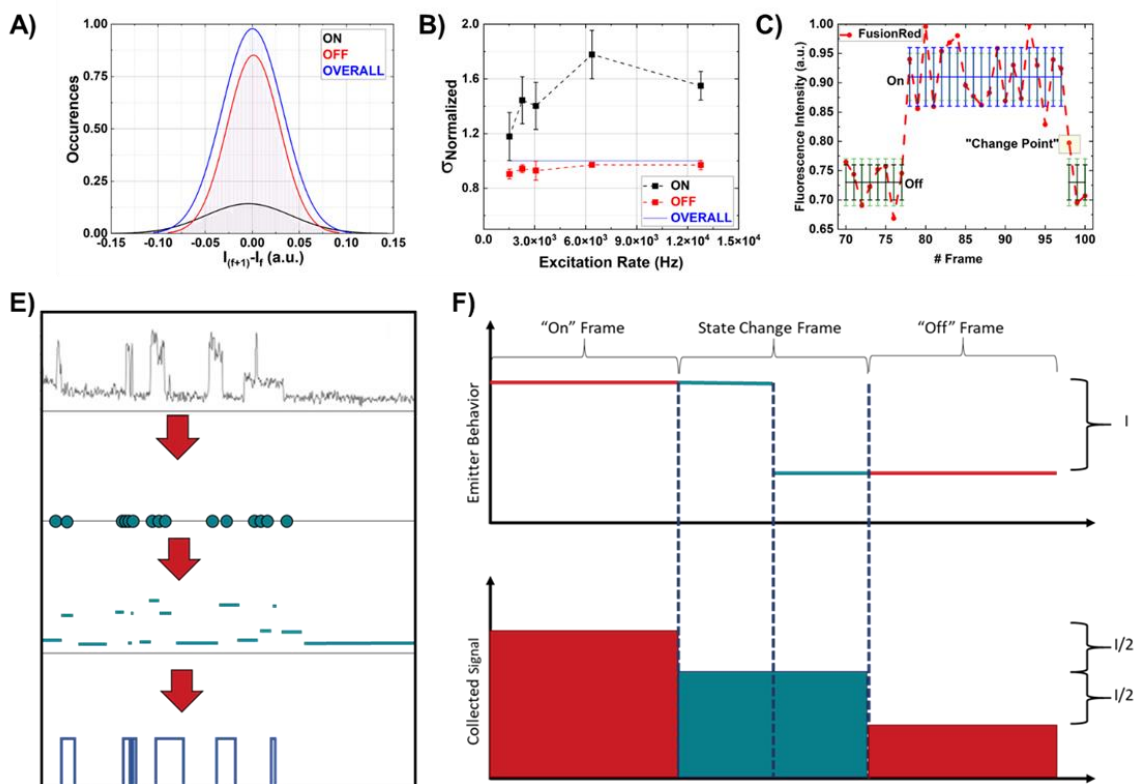
Figure S3.2: Intensity variation: (A) On/ Off and Overall fluctuation histograms, (B) Levels of fluctuations from the on and off state (read and shot noise), (C) Change point definition. (E) The schematic of how the change point algorithm works to binarize traces (F) The reported intensity of a state change frame is expected to be somewhere between the maximum expected intensity (I) and lower threshold of noise, and the intensity change with respect to either the preceding or following frame is expected to be greater than or equal to I/2.

S4. Ensemble photobleaching

Figure S4.1 shows the ensemble bleaching of these two proteins in bacteria.
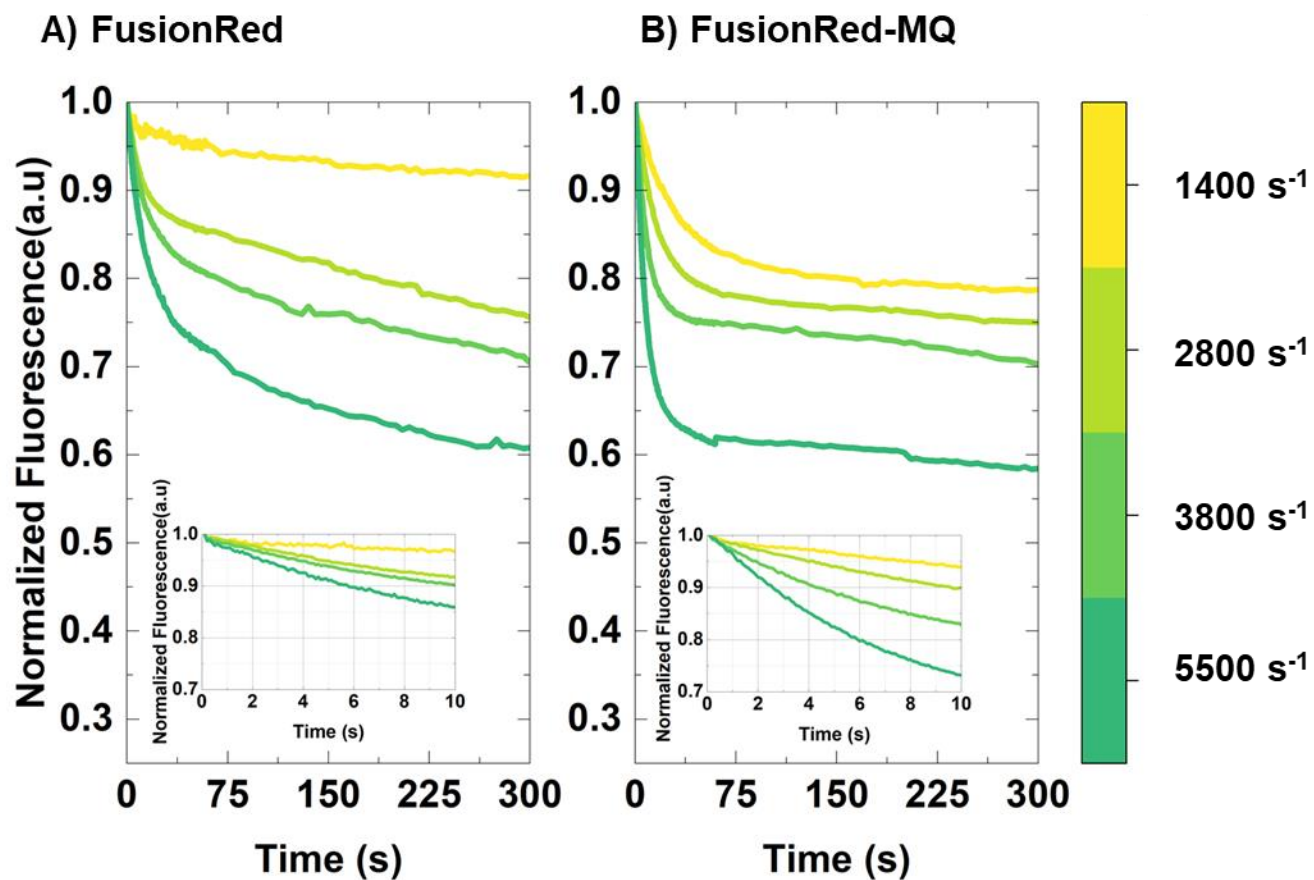
Figure S4.1: Photobleaching traces of *E.coli* expressing (A) FusionRed and (B) FusionRed-MQ, across varying irradiance ranges.
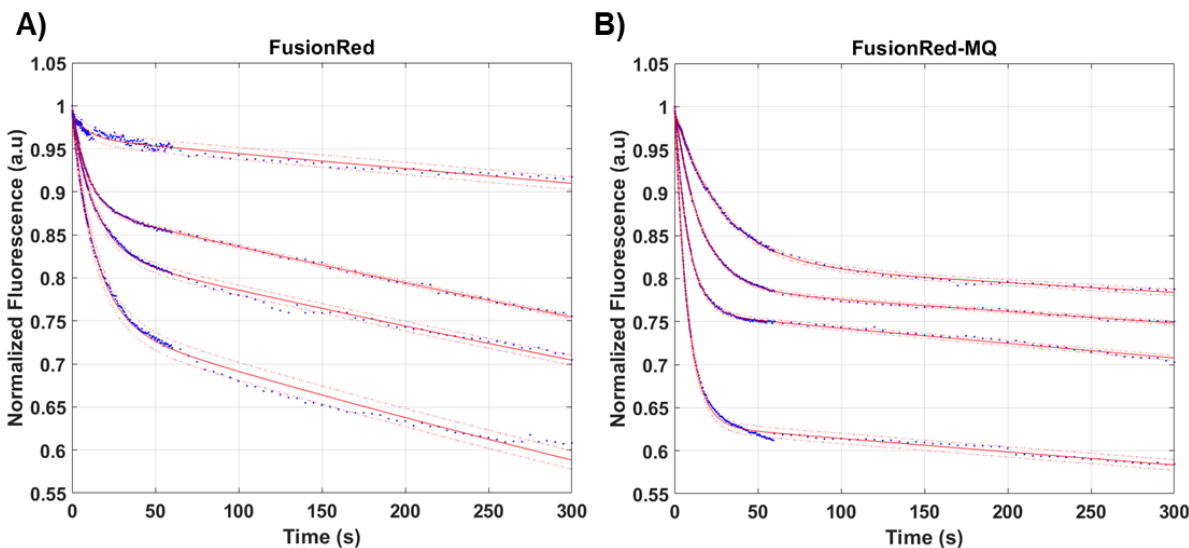
Figure S4.2: Bi-exponential nature of fluorescence decay from bacteria expressing FusionRed and FusionRed-MQ.

Table S4.1: Fitting details for the biexponential decay traces of FusionRed and FusionRed-MQ

k_{Ex} (s^{-1})	FusionRed				FusionRed-MQ			
	τ_1 (s)	A_1 (%)	τ_2 (x10^3 s)	A_2 (%)	τ_1 (s)	A_1 (%)	τ_2 (x10^3 s)	A_2 (%)
1400	14.1 ± 2.4	2	5.4 ± 0.3	97	27.9 ± 0.5	16	7.1 ± 0.3	84
2800	12.6 ± 2.2	12	2.4 ± 0.6	88	15.6 ± 0.1	21	5.6 ± 0.1	79
3800	9.4 ± 1.8	16	1.8 ± 0.1	84	8.2 ± 0.1	24	4.1 ± 0.1	76
5500	9.9 ± 2.6	24	1.6 ± 0.6	76	7.7 ± 0.1	34	3.4 ± 0.1	66

The bleaching curves were fit to a biexponential function $f(t)=A_1e^{-k1t}+A_2e^{-k2t}$ to provide a quantitative estimation of the time constants that are representative of the permanent and the reversible photobleaching. In both cases, the larger time constant τ_2 is ~100-500-fold larger than the shorter τ_1. Consequently, we attribute τ_2 to permanent photobleaching and τ_1 to reversible photobleaching. With increasing irradiance, we observe accelerated photobleaching for both FPs and their respective time constants. These measurements are in line with simulations presented in Figure S5.6, where an increase in the dark fraction (or A_1) is observed with increments in irradiances. For the relevance of this study, we will focus on the faster component of photobleaching, which provides a starting point for estimating rate-constants for simulations and for fitting protocols to extract experimental DSC rate constants.

S5. Simulations

Theory and methodology: The processes resulting from perturbation of an FP with visible light can be illustrated by a simple 3-state model as briefly described in the body and Figure 1 of the main text.

Based on this model the molecular brightness (B) from fluorescence of an FP is simply given by,

$$B = \varepsilon \times \phi$$

where ϕ is the fluorescence quantum yield and ε is the extinction coefficient ϕ is the fraction of photons emitted compared to photons absorbed, and thus a measure of the extent to which non-radiative processes contribute to depopulation of the excited state. The extinction coefficient is representative of the one-photon absorption cross section (σ) of the FP molecule, and is a wavelength-dependent constant representing the capacity of the fluorophore to absorb resonant electromagnetic radiation.

In this model, at room temperature, the majority of FP chromophores occupy the ground electronic state (S_0), as dictated by the Boltzmann distribution. Upon absorption of a resonant photon, a transition occurs to the first excited state (S_1), directly dependent on σ. From here the molecule can either relax directly to the S_0 by emitting a photon (fluorescence), or non-radiatively by internal conversion. The system might also undergo a non-radiative transition to a dark state (D) (or other reversible or permanent dark states). The chemical nature of the D varies with different fluorophores. We have described the many competing mechanisms identified in FPs in the introduction section of the main text. Thus, a single fluorophore can also exhibit multiple competing dark states that can be dependent on the irradiance or any other physical parameter like the wavelength of light used (as seen for the irradiance dependence of DSC observed for FusionRed-MQ).

To simplify our model, we assume a single D and the non-radiative transition from S_1 to D is here addressed as the dark state conversion (DSC) process, and non-radiative relaxation from D to S_0 is called ground state recovery (GSR) process. It should be noted that vibrational relaxation to the lowest vibrational level of each molecular energy level also occurs; however, the timescale for such vibrational relaxation is typically fast compared to other transitions, so this process is neglected in our simulations and measurements. Additionally, based on previous high irradiance experiments performed by Manna et. al (JPC-B; 2015) – we assumed DSC 10^2-10^4 – fold faster than the GSR.[3] At the ensemble level, the presence of a dark state leads to a fast decay component in the measured fluorescence, as the excited state population decreases due to DSC. This makes GSR the rate determining step of the fast decay time, i.e. the first component of photobleaching presented in Table S4.1 is dominated by the GSR process, as it is assumed to be significantly longer than the DSC process. This further provides ground to extract τ_{DSC} (by fixing τ_{GSR}) using fitting ensemble bleaching curves presented in Supplementary Information S7.

At the single-molecule level, the presence of a dark state results in the blinking phenomenon, where the cycle of excitation and emission between S_0 and S_1 (the "on" state) is interrupted by a transition to D (the "off" state). During irradiation, the cycle of excitation, emission, internal conversion, dark state conversion, and ground state recovery continues until the fluorophore undergoes an irreversible conformational change or reaction to a state which can no longer fluoresce. This process is termed irreversible photobleaching, which can take place from both the S_1 and the dark state. We neglect the bleaching from the S_1 as we observe a significantly longer second time constant τ_1 as reported in Table S4.1. Under low irradiances employed in these experiments, the fraction of molecules in the S_1 can be expected to be small and light-driven higher-order non-linear photobleaching can also be assumed to be negligible. We can also discount the dark state bleaching for this model, as we previously assumed that that vibrational relaxation to the lowest vibrational level of each molecular energy level is fast, and the D to S_0 GSR process is dominated

by climbing a barrier between trans and cis conformations of the chromophore in the ground electronic state manifold. (Figure 7; Main Text). Finally, as we are not in the regime of optical saturation of the electronic transition ($\sim 10^8$ photons/s or $> kW/cm^2$) – the probability of accepting a photon in the S_1 or the D states is very low. This allows us to assume rate constants that involve stimulated emission, transition to higher order electronic states (S_2 and beyond), reversible conversion from the D to the S_1 state negligible.

With this devised model, for low excitation rate single molecule imaging methods such as widefield and TIRF, we devise a Monte-Carlo algorithm with simulation acquisition time step Δt being longer than excited state lifetime but shorter than GSR time typical for single molecule methods like SOFI (~ 100 ms). This allows us to assume that the FP is in S_0 or D, and invoke a steady-state approximation on S_1 (as it is only a temporary state). The fluorophore starts from either S_0 or D and returns to S0 or D in each time cycle, and rate constants for emission, DSC and GSR decide the probability to change a state during this cycle. This is based on the probability that at a certain timestep a state change takes place when a random number satisfies a given condition (greater or less than) for an event with probability $p(t)= \exp(-\beta k_1(t))$. The code has been made freely available with other analysis codes on GitHub at: https://github.com/srijit2207/FR_DarkState.git.

In the next few pages, we report the simulations performed to bolster our experimental data on single molecules and ensembles.

Simulation Results:

a. On/Off time dependence on DSC and GSR times and excitation rates
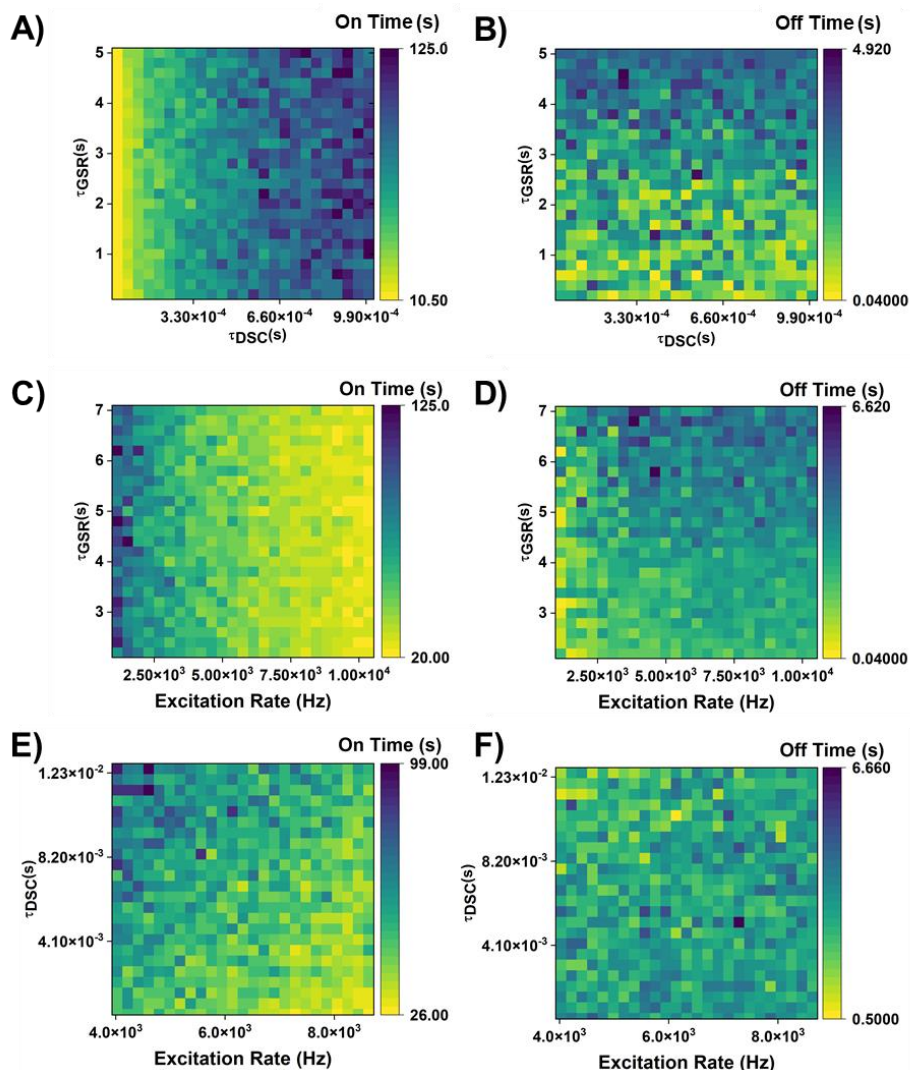
Figure S5.1: Variations of on and off times with respect to τ_{DSC} (=1/k$_{DSC}$) and τ_{GSR} (=1/k$_{GSR}$) expected from simulations. (A and B) Variation of on and off times with DSC and GSR times at a fixed excitation rate (1923 Hz). (C and D) Variation of on and off times with excitation rate and GSR times at a fixed DSC time (0.5 ms). (E and F) Variation of on and off times with excitation rate and DSC times at fixed GSR time (3 s). We observe a shorter on-time for both shorter dark-state conversion times and higher excitation rates (Figure S5.1, Panels A, C and E). We also observed that off-times depend only on the ground-state recovery times (Figure S5.1, Panels B, D and F). The heatmaps represent the variation of on and off times, with blue being higher values and yellow being lower values. Each pixel on the histogram represents an average on/off lifetime (τ_{ON}/ τ_{OFF}) obtained from histograms of individual on and off segments for 150 simulated blinkers. The photophysical properties used for the simulation (extinction coefficient, absorption and emission spectra, fluorescence quantum yield and fluorescence lifetime) were of FusionRed. The values can be found in our previous publication.[2] The DSC and GSR times were estimated from the time constant of the reversible bleaching presented in Figure S4.1 and for our previous high-irradiance measurements for mCherry, Kreik and TagRFP-T.[3]

b. Effects of changing time steps on this algorithm

This model considers the time step to be longer than the excited state lifetime and the dark state conversion time but slower than the ground state recovery time. This is done to mimic millisecond acquisition times for commercial EMCCD and CMOS cameras employed for single molecule imaging. We ignore photobleaching in these simulations. We used $\tau_{DSC} \cong 40$ µs, $\tau_{GSR} \cong 2$ s, $\Phi \cong 0.24$, $\tau_{FL} \cong 1.78$ ns and $k_{ex} \cong 3500$ Hz for these simulations.

Case 1: One FusionRed protein, image acquisition time 100 ms, 6000 frames.
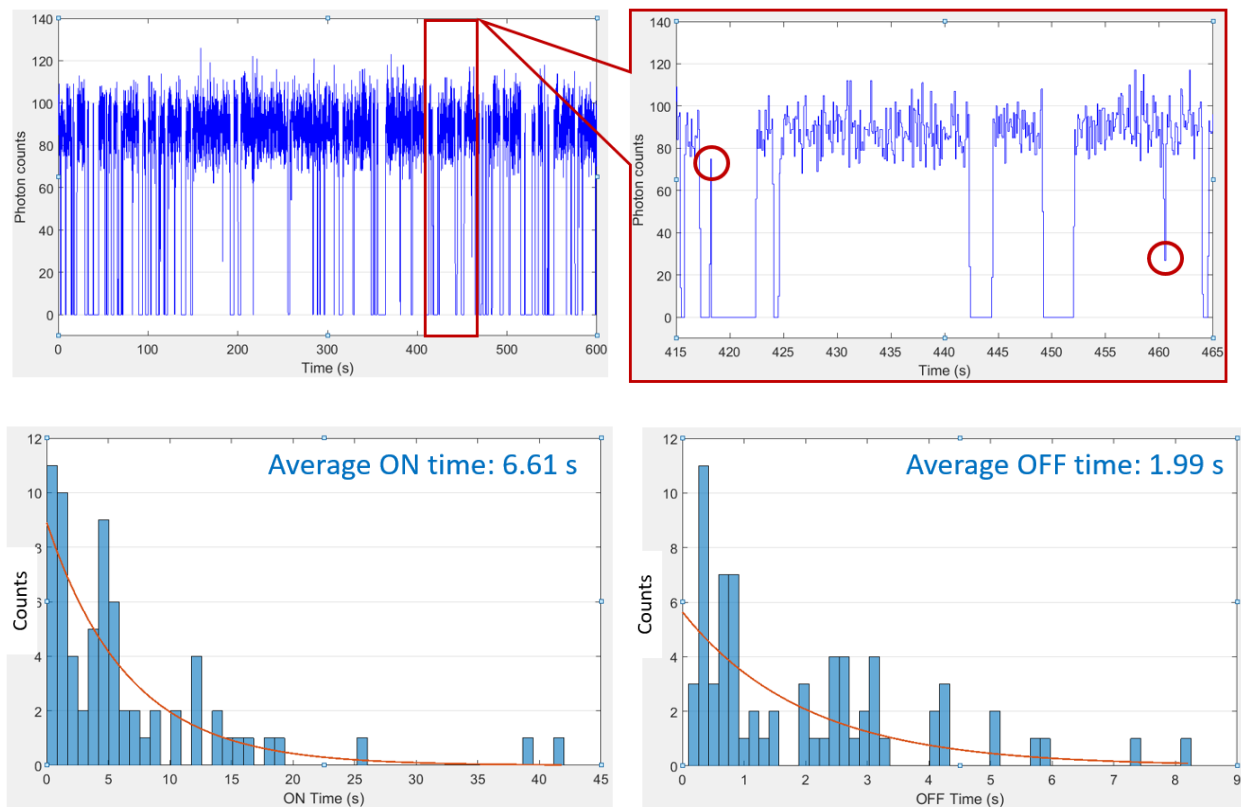
Figure S5.2: (Above) Single molecule trajectories. The red circles indicate frames where photon counts are lower than most on events, indicating the switching off of the molecule mid-frame of the acquisition step. Our single molecule binarization change-point algorithm can recognize these real fluctuations and jumps and distinguish these from experimental background noise. (Below) The histograms of binarized on and off traces.

Case 2: One FusionRed protein, image acquisition time 50 ms, 12000 frames.
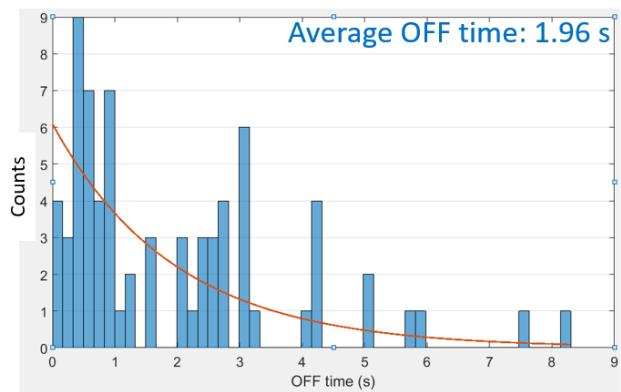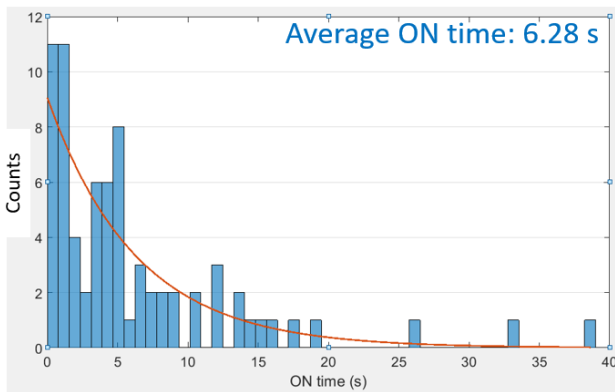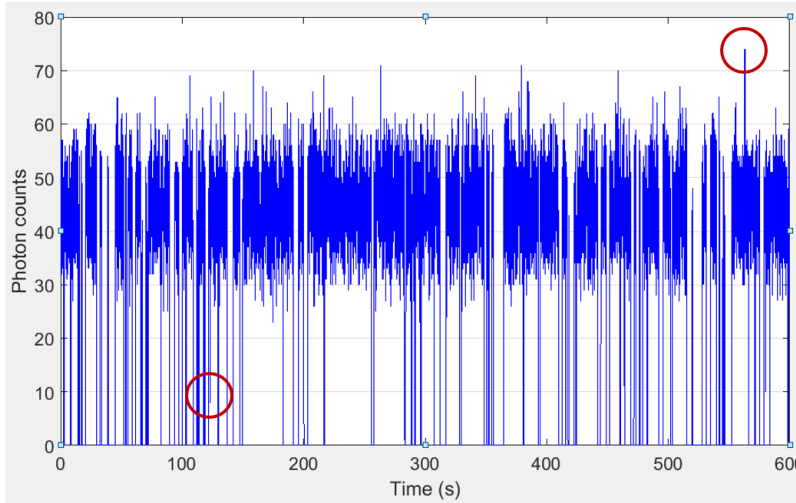
Figure S5.3: (Above) The photon count on the camera reduces by ~50% when the acquisition time is halved. (Below) The statistics of on and off times do not change on changing the frame rate.

Similarly, when the image acquisition time is reduced to 20 ms, the photon counts also reduce accordingly, but the on/off times are similar to the above two cases.

c. Statistics of on/off time for a single FP blinking versus multiple FPs under the same time step

Case 3: Repeat 50 simulations of single FusionRed protein, image acquisition time 50 ms and taking 6000 frames for each FusionRed protein simulation. In comparison to case 2 presented in the previous simulation.
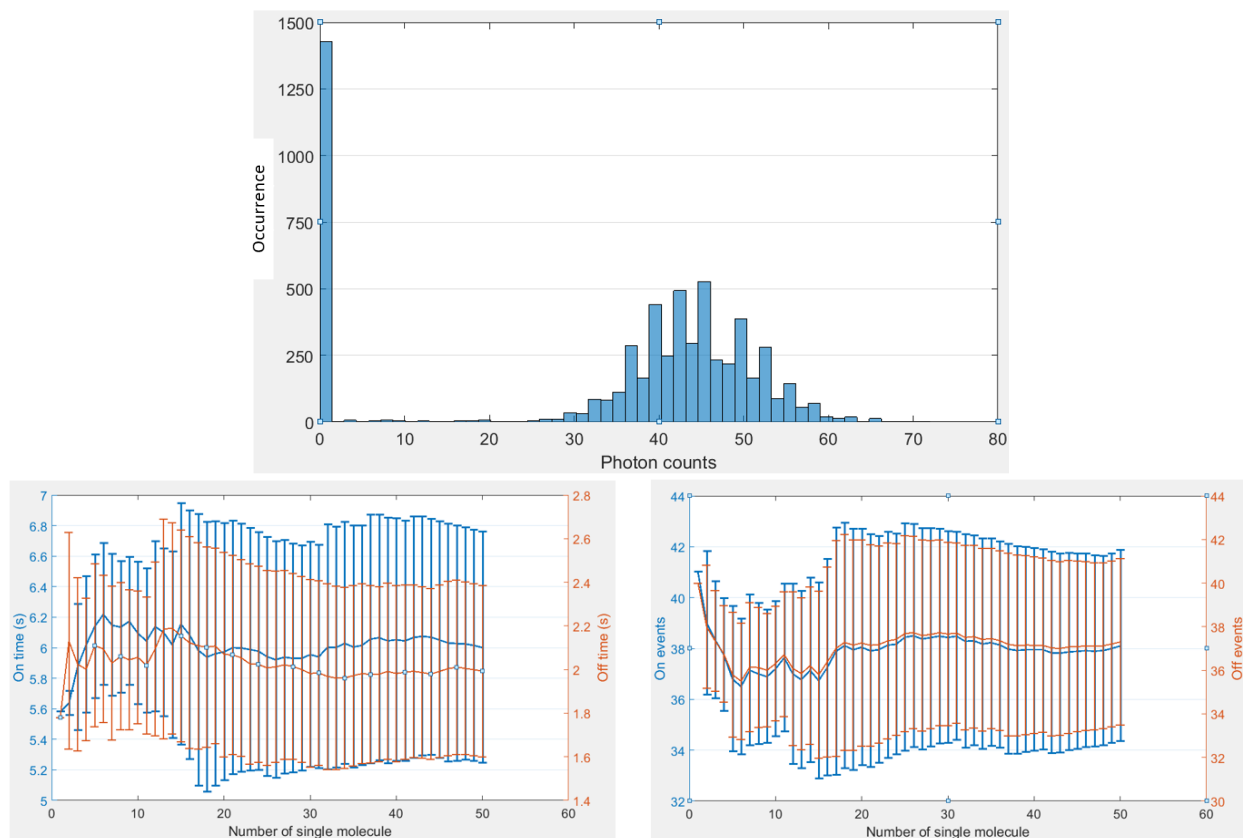
Figure S5.4: (Above) The photon count histograms are centered at ~45 photons for either case. (Below) The fluctuations for on and off times become relatively consistent after ~5 FPs.

The on/off statistics do not change as the photon counts drop. We still remain below the optical saturation limit and observe near linear photon counts.

d. Statistics of on/off time relevant to an actual single molecule experiment

Our experiments were carried out using camera acquisition times of ~100–300 ms for 50–500 FPs. This case describes the simulated data for these settings.

Case 4: In total, 50 simulations of single FR proteins, image acquisition time 300 ms and taking 1000 frames for each FR protein simulation (~5-minute trajectories).

Photon count distribution is shifted ~6 times higher than Case 3, since the acquisition time is 6 times longer. The average ON/OFF time and number of ON/OFF events are also shown below. The average ON/OFF time is slightly longer than Case 3 because the ON/OFF time is added in the unit of the image acquisition time. The average number of ON/OFF events observed in this case are slightly less than Case 3, also because of the longer acquisition time, i.e., the shorter the acquisition time, the more the ON/OFF switching events can be observed. However, the number of events does not change significantly since the average ON/OFF times are much longer than the acquisition time.
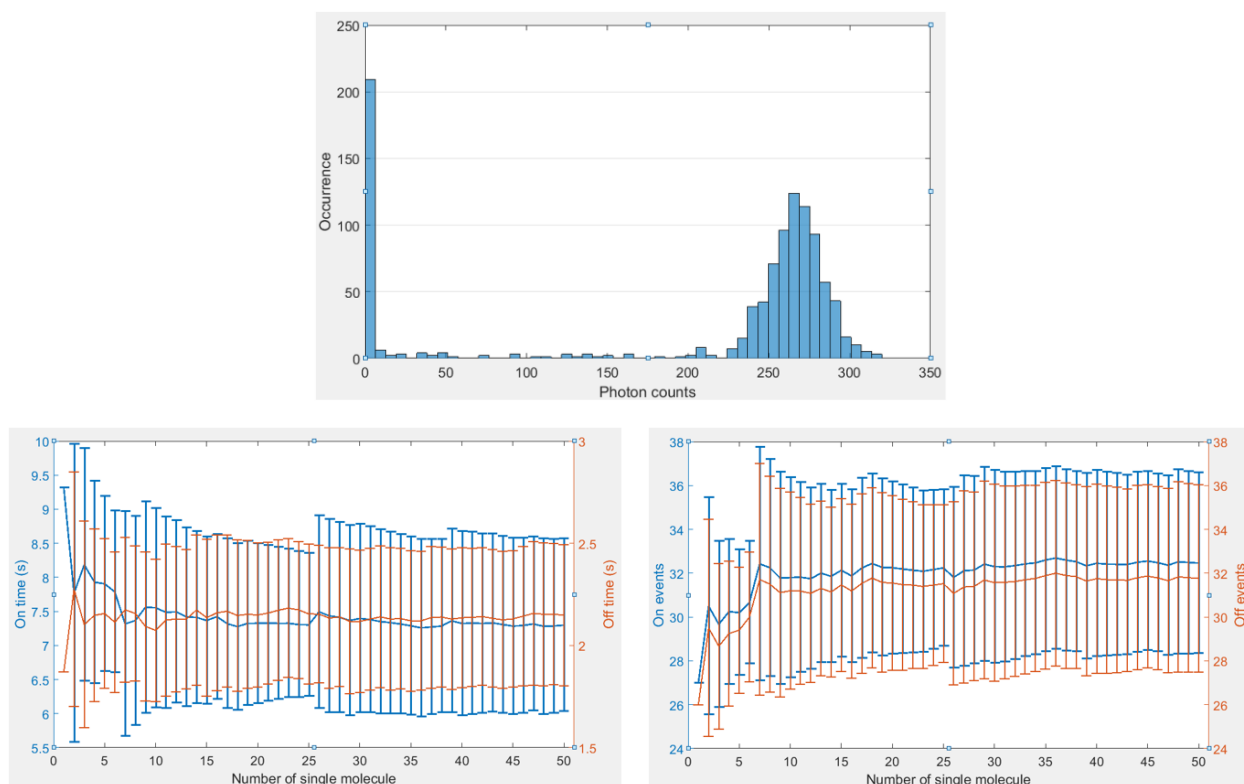
Figure S5.5: (Above) At 300 ms, our photon counts are significantly higher than at shorter acquisition time. (Below) The fluctuations for on and off times are almost consistent after ~5 FPs.

e. Ensemble behavior averaged from simulated single molecule blinking with respect experimental rate constants obtained from experiments.
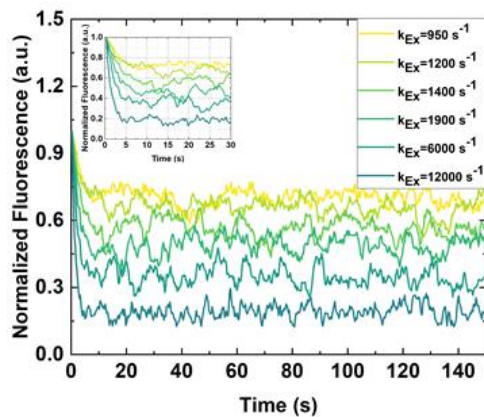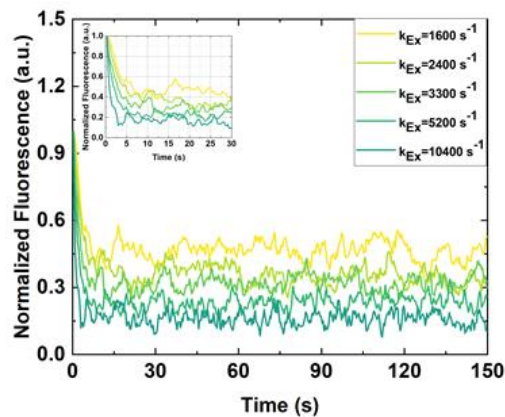
Figure S5.6: Ensemble trends from Monte-Carlo simulations obtained from rate constants reported in Main Text Table 2, without permanent photobleaching. FusionRed-MQ shows a larger dark fraction and faster dark state conversion in comparison to FusionRed. Each trace represents the normalized sum fluorescence from three simulated single molecule blinking video with ~150 emitters.

f. Simulation of ensemble behavior averaged from simulated single molecule blinking with respect to varying k_{Ex}, k_{DSC} and k_{GSR} while holding other rate constants fixed.
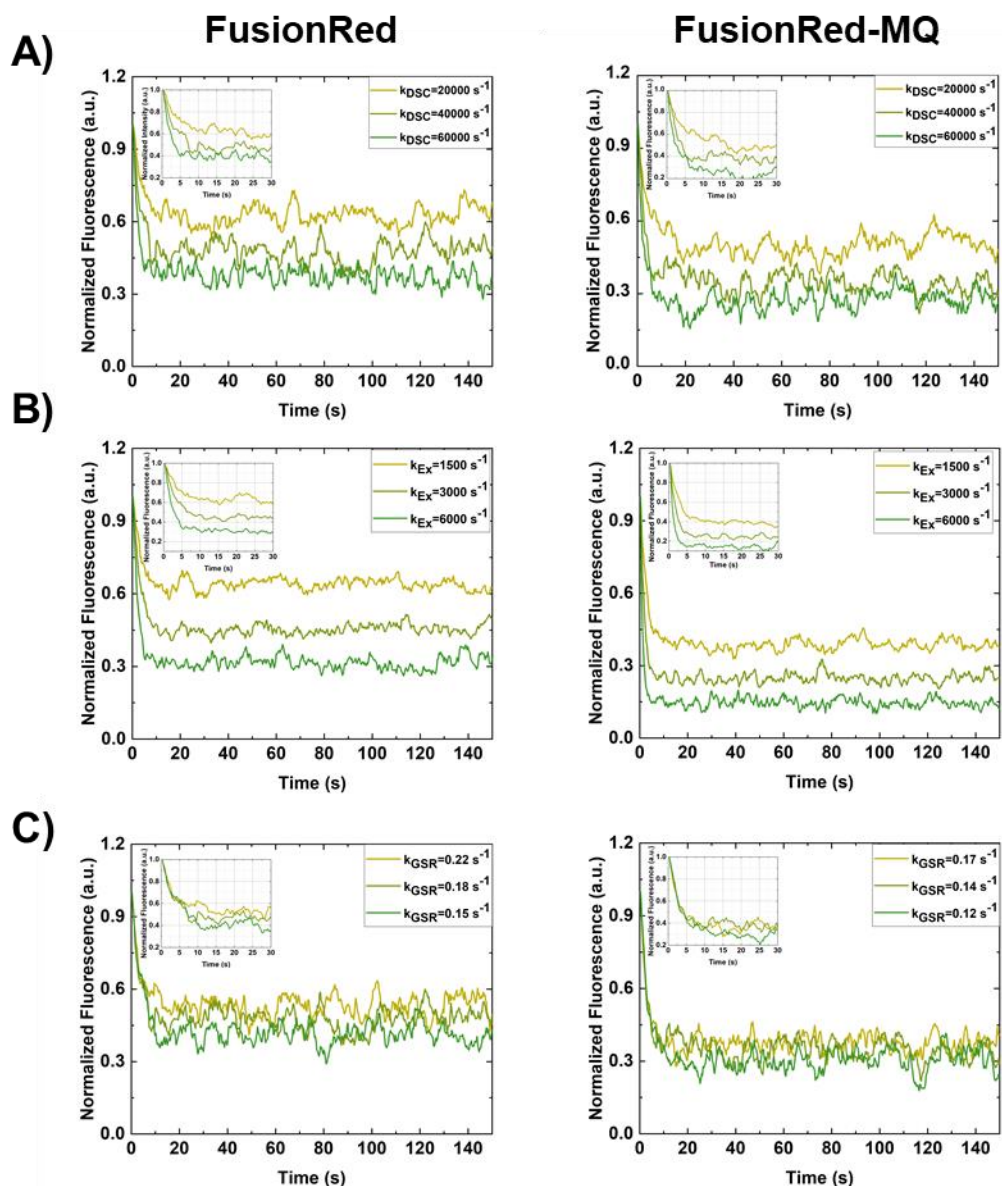
Figure S5.7: Variation in fluorescence decay traces with respect to k_{DSC}, k_{ex} and k_{GSR}. Each trace represents the normalized sum fluorescence from three simulated single molecule blinking videos, each with ~150 emitters. The panel on the left represents the simulated traces with respect to photophysical properties of FusionRed and on the right, photophysical properties of FusionRed-MQ. For each panel, the one rate constant was varied at a time while keeping the other two rate constants fixed, for example – for FusionRed panel A, k_{DSC} was varied keeping $k_{ex}=3000$ s^{-1} and $k_{GSR}=0.18$ s^{-1} fixed. These results provide insight into how each rate constant involved in dark state population and depopulation manifest at an ensemble level.

g. Ensemble behavior of the system based on numerical simulations for a three-state system
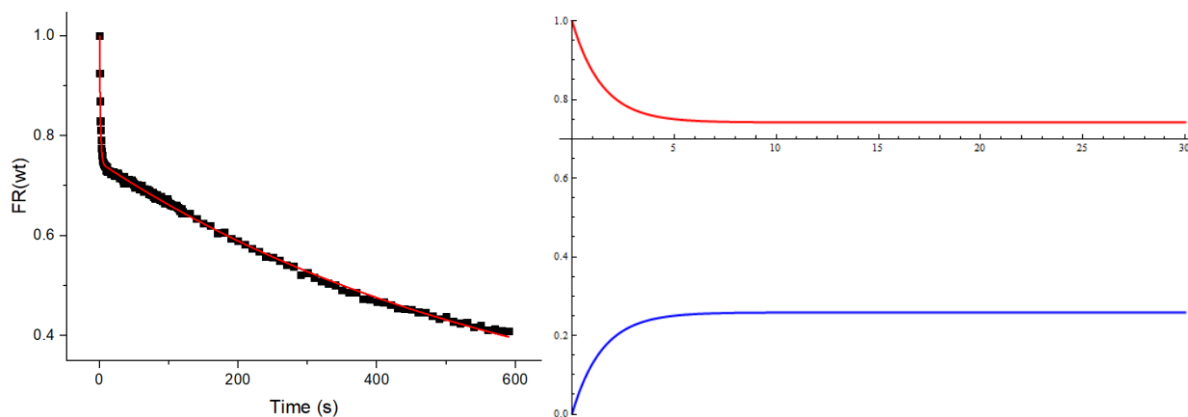
Figure S5.8: A population based numerical simulation (non-Monte Carlo methods) indicates that the k_{DSC} controls the dark fraction at the ensemble level. (Left) Photobleaching curve of FusionRed fit with two exponential functions. (Right) Normalized populations in S_0 (red) and D (blue) over time (x axis, in seconds) without considering permanent photobleaching obtained from by utilizing rate constants from these fit on the left and numerical simulations for a three-state model.

S6. Statistical testing

The average k_{GSR} and k_{DSC} across irradiances for FusionRed and FusionRed-MQ were subject to statistical testing to indicate if the differences between the two average values were significant or not.

- *2-tailed independent t-test for k_{GSR}:*

  k_{GSR} (FR)= 0.195 ± 0.012 Hz

  k_{GSR} (FR-MQ) = 0.154 ± 0.005 Hz

  DOF=11-2=9

  t_{Crit}=7.64 > $t_{P=0.05}$=2.26

  Null hypothesis rejected, **means are from two different distributions**

- *2-tailed independent t-test for k_{DSC}:*

  k_{DSC} (FR)= 52 ± 11 kHz

  k_{DSC} (FR-MQ) = 44 ± 6 kHz

  DOF=11-2=9

  t_{Crit}=1.68 > $t_{P=0.05}$=2.26

  Null hypothesis accepted, **means are from the same distribution**

S7. Additional fitting results

a. Analytical expression for fitting the ensemble fluorescent population:

Three-state model equation: $S_0(t) = A * k_{DSC} * (4 * k_{GSR} * (k_{DSC} + k_{Em} + k_{IC}) * sqrt ((k_{DSC} + k_{Em} + kEx + k_{GSR} + k_{IC})^2 - 4 * (k_{DSC} * (k_{Ex} + k_{GSR}) + k_{GSR} * (k_{Em} + k_{Ex} + k_{IC}))) + exp (- 0.5 * t * (k_{DSC} + k_{Em} + k_{Ex} + k_{GSR} + k_{IC} + sqrt ((k_{DSC} + k_{Em} + k_{Ex} + k_{GSR} + k_{IC})^2 -4 * (k_{DSC} * (k_{Ex} + k_{GSR}) + k_{GSR} * (k_{Em} + k_{Ex} + k_{IC}))))) * k_{Ex} * (k_{DSC} + k_{Em} + k_{Ex} + k_{GSR} + k_{IC} - sqrt ((k_{DSC} + k_{Em} + k_{Ex} + k_{GSR} + k_{IC})^2 - 4 * (k_{DSC} * (k_{Ex} + k_{GSR}) + k_{GSR} * (k_{Em} + k_{Ex} + k_{IC})))) * (- k_{DSC} + k_{Em} + k_{Ex} - k_{GSR} + k_{IC} + sqrt ((k_{DSC} + k_{Em} + k_{Ex} + k_{GSR} + k_{IC})^2 - 4 * (k_{DSC} * (k_{Ex} + k_{GSR}) + k_{GSR} * (k_{Em} + k_{Ex} + k_{IC})))) - exp (0.5 * t * (- k_{DSC} - k_{Em} - k_{Ex} - k_{GSR} - k_{IC} + sqrt ((k_{DSC} + k_{Em} + k_{Ex} + k_{GSR} + kIC)^2 - 4 * (k_{DSC} * (k_{Ex} + k_{GSR}) + k_{GSR} * (k_{Em} + k_{Ex} + k_{IC}))))) * k_{Ex} * (- k_{DSC} + k_{Em} + k_{Ex} - k_{GSR} + k_{IC} - sqrt ((k_{DSC} + k_{Em} + k_{Ex} + k_{GSR} + k_{IC})^2 - 4 * (k_{DSC} * (k_{Ex} + k_{GSR}) + k_{GSR} * (k_{Em} + k_{Ex} + k_{IC})))) * (k_{DSC} + k_{Em} + k_{Ex} + k_{GSR} + k_{IC} + sqrt ((k_{DSC} + k_{Em} + k_{Ex} + k_{GSR} + k_{IC})^2 - 4 * (k_{DSC} * (k_{Ex} + k_{GSR}) + k_{GSR} * (k_{Em} + k_{Ex} + k_{IC}))))) / (4 * (k_{DSC} * (k_{Ex} + k_{GSR}) + k_{GSR} * (k_{Em} + k_{Ex} + k_{IC})) * sqrt ((k_{DSC} + k_{Em} + k_{Ex} + k_{GSR} + k_{IC})^2 - 4 * (k_{DSC} * (k_{Ex} + k_{GSR}) + k_{GSR} * (k_{Em} + k_{Ex} + k_{IC})))) + A_{PB} * k_{PB} + C_{Offset}$

b. Inaccuracies in fitting the ensemble bleaching with a fixed dark-state conversion rate constant:
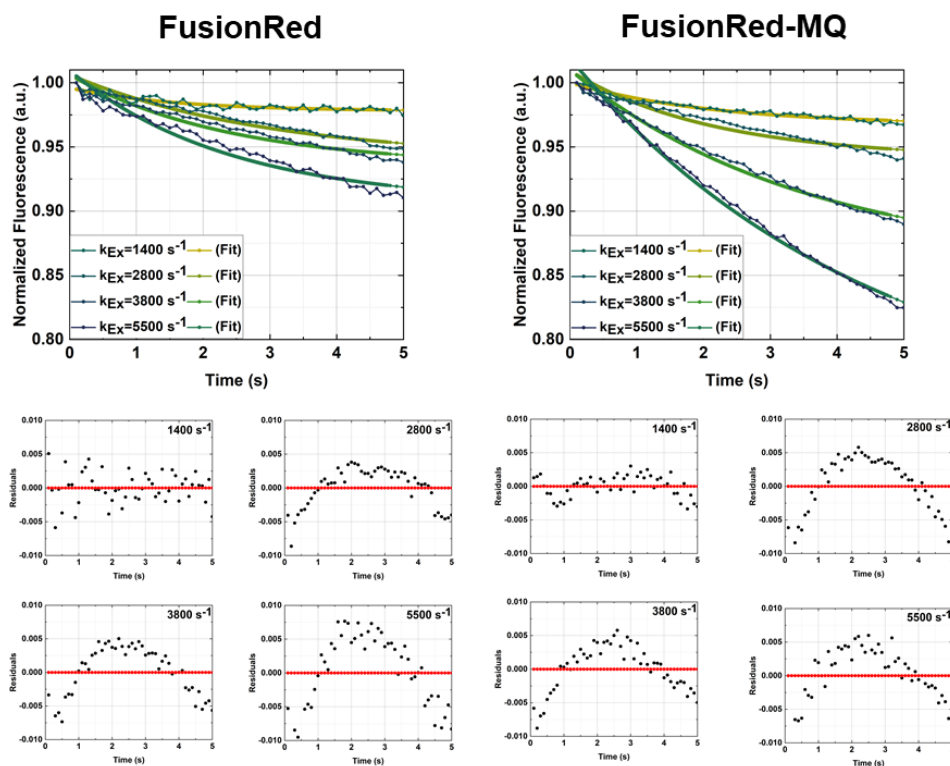
Figure S7.1: Quality of fit for varying k_{DSC} and k_{GSR} unbound. Residuals indicate a poor quality of fitting. Since single-molecule experiments provide precise measurements for the GSR in comparison to DSC, fixing the k_{GSR} within the experimental bounds of the single-molecule measurement and then fitting for k_{DSC} provided better insight and accurate estimation of the kinetics for the dark-state conversion process.

c. **Residuals for fitting k$_{DSC}$ with respect to a bound value of k$_{GSR}$**
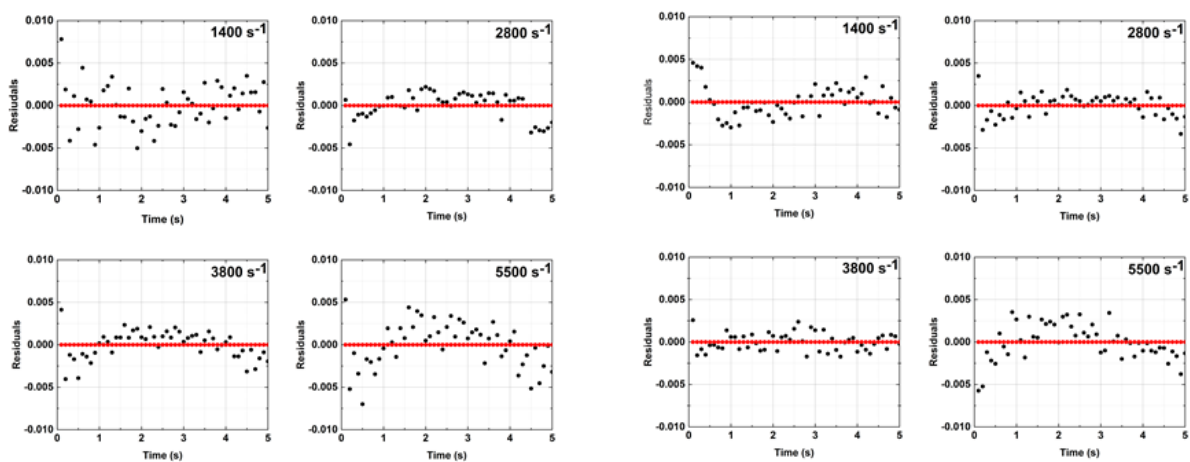
Figure S7.2: Keeping fixed k$_{GSR}$ while allowing the fitting algorithm to fit the k$_{DSC}$ provides better quality of fit. Residuals indicate better fitting, with adj-R^2 > 0.95.

S8. Theoretical estimation of the lowest and highest number of photons per frame

Lower bound: Lowest excitation rate for FusionRed

k_{ex} = 940 photons/s

Fluorescence QY of FusionRed = 0.24

Total fluorescence photons = 226 photons/s

Acquisition time = 300 ms, Quantum Efficiency[4] of Andor iXon at 561 nm ~0.8

Maximum number of fluorescence photons per frame ~60 photons/ frame

Numerical aperture of objective ~ 1.42

% light collected by the objective ~ 0.4

Realistic lower bound ~ **25 photons/ frame**

Upper bound: Highest excitation rate for FusionRed-MQ

k_{ex} = 20800 photons/s

Fluorescence QY of FusionRed = 0.43

Total fluorescence photons = 8950 photons/s

Acquisition time = 300 ms, Quantum Efficiency[4] of Andor iXon at 561 nm ~0.8

Maximum number of fluorescence photons per frame ~2300 photons/ frame

Numerical aperture of objective ~ 1.42

% light collected by the objective ~ 0.4

Realistic upper bound ~ **900 photons/ frame**

S9. Surface charge on FusionRed
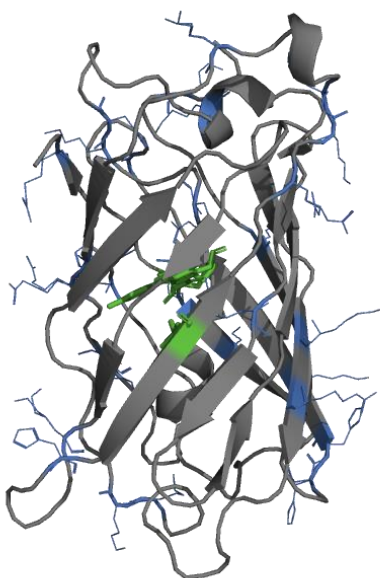
Figure S9.1: The crystal structure of FusionRed (PDB ID: 6U1A) indicating the location of positively charged amino acid sidechains pointing out of the β-barrel (blue lines). These provide the opportunity to effectively bind the molecule with a negatively charged glass surface. The mutations acquired in FusionRed-MQ point into the barrel facing the chromophore (green). Therefore, we expect similar perturbations in FusionRed and FusionRed-MQ with respect to electrostatic interactions of the glass surface for both FPs.

References:

1. M. L. Martin-Fernandez, C. J. Tynan and S. E. D. Webb, A 'pocket guide' to total internal reflection fluorescence, *J. Microsc.*, 2013, **252**, 16–22.

2. S. Mukherjee, S. T. Hung, N. Douglas, P. Manna, C. Thomas, A. Ekrem, A. E. Palmer and R. Jimenez, Engineering of a brighter variant of the FusionRed fluorescent protein using lifetime flow cytometry and structure-guided mutations, *Biochemistry*, 2020, **59**, 3669–3682.

3. P. Manna and R. Jimenez, Time and frequency-domain measurement of ground-state recovery times in red fluorescent proteins, *J. Phys. Chem. B*, 2015, **119**, 4944–4954.

4. R. van den Eynde, A. Sandmeyer, W. Vandenberg, S. Duwé, W. Hübner, T. Huser, P. Dedecker and M. Müller, Quantitative comparison of camera technologies for cost-effective super-resolution optical fluctuation imaging (SOFI), *JPhys Photonics*, 2019, **1**, 44001.